Journal of Science and Technology in Civil Engineering, HUCE, 2023, 17 (4): 48–65

FLEXURAL-SHEAR STRENGTHENING OF REINFORCED CONCRETE T-BEAMS SUBJECTED TO ASYMMETRIC LOADING USING CFRP SYSTEM COMBINED BY NSM STRIPS AND U-WRAPS

Nguyen Dang Nguyen[a], Dang Tung Lam[a], Nguyen Ngoc Tan[a,*]

[a] *Faculty of Building and Industrial Construction, Hanoi University of Civil Engineering, 55 Giai Phong road, Hai Ba Trung district, Hanoi, Vietnam*

Article history:
Received 05/10/2023, Revised 19/12/2023, Accepted 19/12/2023

Abstract

This paper presents a developed three-dimensional (3D) finite element model (FEM) of flexural and shear strengthening of reinforced concrete (RC) T-beams using a CFRP (Carbon Fiber-Reinforced Polymer) system combined by near-surface mounted (NSM) strips and U-wraps subjected by asymmetric loading. The 3D FEM was verified by experimental results. Concrete was simulated by a total-strain-based rotating smeared crack model. NSM CFRP strips and CFRP U-wrap sheets were modeled as shell elements. Steel reinforcement and NSM CFRP strips were embedded in concrete, corresponding to a perfect bond. U-wrap sheets were modeled as a shell element and bonded to the concrete surface using an interface element, considering appropriate bond properties. Four RC T-beams from an experimental work were analyzed, and predictions of the applied load-displacement curve and failure mode were presented to demonstrate the accuracy of the developed finite element analysis. It is shown that the finite element results of T-beams agree well with the experimental behavior in terms of applied load versus displacement and failure mode. Moreover, a parametric study was conducted to examine the influence of some design-oriented parameters such as concrete compressive strength, amount of longitudinal tension reinforcement, amount of stirrups, multiple layers of externally bonded (EXB) CFRP sheets, and flange width.

Keywords: T-beams; flexural-shear strengthening; carbon fiber-reinforced polymer; asymmetric loading; finite element analysis (FEA).

https://doi.org/10.31814/stce.huce2023-17(4)-05

1. Introduction

Existing structures, especially RC beams, are designed and constructed according to the requirement of the obsolete design code and may have insufficient detailing and amount of longitudinal reinforcements and stirrups. RC structures may also undergo corrosion of steel reinforcement after a certain year in service. Due to corrosion, the bearing capacity and stiffness of existing RC beams could be adversely affected [1, 2]. Because of those reasons, RC beams could fail in shear, which is a brittle failure mode, without warning for people who might escape. Those beams may be repaired or strengthened for some reasons such as (1) repairing existing damage to achieve better performance, (2) compiling with updated requirements in modern design codes when changing the function of the building, and (3) satisfying the building owner's concern about human safety and property protection. The existing RC beams must be thoroughly analyzed to determine the bearing capacity, considering the building's functions and aesthetics. Strengthening solutions involve the use of new materials that are different from those of the original material. Furthermore, the interactions of those materials

*Corresponding author. *E-mail address:* tannn@huce.edu.vn (Tan, N. N.)

must be well understood. The selected strengthening solution must be economically and technically feasible.

Under such circumstances, CFRP material has emerged as a new material that attracts much attention for repairing and strengthening structures. CFRP material has some outstanding features such as low volumetric mass, high strength-to-weight ratio, high tensile strength, high corrosion resistance, and simple construction procedures, which can save the costs associated with material transportation and on-site construction [3–5]. Consequently, construction time can be reduced without much impact on structural integrity. Owing to its high tensile strength, CFRP is often used to enhance the bearing capacity of RC beams and slabs [6–8].

It may be necessary for an existing RC beam to increase the bending and shear load-carrying capacity simultaneously. In order to avoid the shear failure of an RC beam, the beam needs to strengthen its shear resistance when its shear capacity drops below its flexural capacity after flexural strengthening applications have been submitted. Given this situation, it is essential to develop an effective CFRP strengthening solution that addresses both flexural and shear strengthening. Some useable techniques of CFRP installation have now been developed, including direct wrapping around a structural member [9], deep embedment method [10] near-surface mounted [11], and externally bonded reinforcement (EBR) or U-wrapping [12]. This paper focuses on the last two: NSM and EBR techniques. EBR is the technique requiring the CFRP (wet lay-up sheets or strips) to be glued using an epoxy resin adhesive to the external faces of the strengthened element. NSM is the technique where CFRP strips (circular, square, or rectangular cross-sections) are installed and tightly attached using epoxy adhesive into pre-cut slits opened on the concrete cover of the elements to strengthen.

Most previous studies have been performed for the flexural strengthening of beams [13–15]. Compared to flexural strengthening, there are far fewer studies on shear strengthening of RC beams, and most of them have been carried out on small specimens with a rectangular cross-section. To date, the shear behavior of CFRP-strengthened RC beams, especially those without stirrups, is still a popular topic of interest for researchers [16–20]. The level of improvement in the shear capacity of beams depends not only on the mechanical properties of the materials used (such as concrete, steel, and CFRP) but also on the amount of CFRP the strengthening techniques [21, 22], and the anchorage techniques [23]. The longitudinal reinforcement and stirrups amounts also significantly influence the shear strength and the crack width, especially the latter [24].

Experimental studies are necessary to observe the actual behavior and failure mode of structural elements. However, experimental studies are often quite expensive in terms of cost and time. As the computation capability of computers increases rapidly, the use of the finite element method to study the behavior of RC structures have developed enormously in recent years [25]. Recently, Tan et al. [18] have successfully constructed 3D finite element models to analyze the shear behavior of RC beams strengthened with CFRP U-wraps subject to a symmetric four-point bending test. Nioko et al. [26] developed a 3D finite element modeling of shear-critical RC beams strengthened with EXB CFRP sheets in a U-wrap configuration.

In the present study, 3D finite element models were constructed and verified for a total of four RC T-beams, including two control beams and two strengthened beams. The strengthened beams were simultaneously reinforced in flexure and shear. Flexural strengthening was applied by NSM CFRP strips, and shear strengthening was implemented by EBR of wet lay-up CFRP sheets of U configuration (abbreviated as EXB CFRP sheets). The beams were subjected to an asymmetric three-point loading test. Material parameters and characteristic results of the mechanical behavior of the beams, such as load-deflection curves, crack patterns, and failure modes, were collected from the

experimental work of Dias et al. [16]. Comparison of the model results with the experimental results confirmed that the 3D finite element models could accurately predict the load-carrying capacity of both the control and strengthened beams, as well as simulate the concrete crack pattern and failure modes such as shear failure and EXB CFRP debonding. A parametric study was then developed to investigate the main parameters affecting the load-bearing capacity of CFRP-strengthened RC T-beams, including (i) concrete compressive strength, (ii) amount of longitudinal tension reinforcement, (iii) amount of stirrups, (iv) number of layers of EXB CFRP sheets, and (v) the flange width.

2. Beam specimens and material constitutive models

2.1. Description of beam specimens

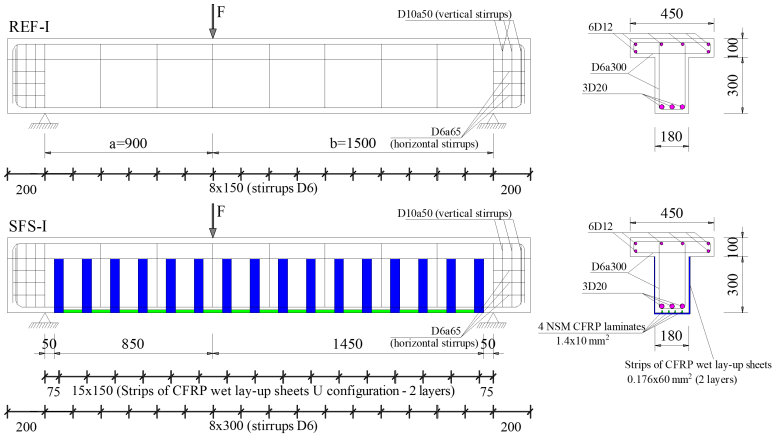

(a) Group I: REF-I and SFS-I

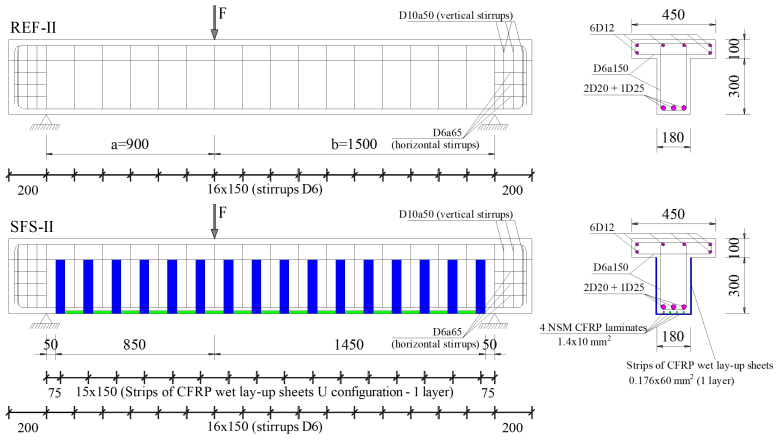

(b) Group II: REF-II and SFS-II

Figure 1. Layout of tested T-beams (dimensions in mm) [16]

In this study, the two groups of RC beams with a T-shaped cross-section taken from the experiments undertaken by Dias et al. [16] were used to verify the reliability of the proposed finite element (FE) model using DIANA [27]. Two beams in each group were selected and analyzed in this work. The two groups differ in the amount of longitudinal tension reinforcements, spacing of stirrups, and the number of layers of the EXB CFRP sheets. Two control beams without CFRP are denoted as REF-I in the first group and REF-II in the second group. Two remaining beams were simultaneously

strengthened for flexure by NSM CFRP strips and shear by EXB CFRP sheets of U shape, designated as SFS-I in the first group and SFS-II in the second group.

The beams had a T-shaped cross-section with a width by the flange depth of 450×100 mm and a width by the web depth of 180×300 mm. The beams were 2800 mm long. It was simply supported with a span of 2400 mm. The beams were subjected to an asymmetric point load with a shear span-to-depth ratio of 2.5, as illustrated in Fig. 1. For all beams, the flange was arranged with six longitudinal bars with a diameter of 12 mm (6D12). The beams were reinforced with three longitudinal bars of 20 mm diameter (3D20) for beam SFS-I, with two longitudinal bars of 20 mm diameter and one longitudinal bar of 25 mm diameter (2D20+1D25) for beam SFS-II. Furthermore, steel stirrups in the 2400 mm length were provided with a 6 mm diameter at 300 mm spacing (D6a300) and 150 mm spacing (D6a150) in the beams SFS-I and SFS-II, respectively. The two beam's ends corresponding to 200 mm length from the supports were designed by D6a65 as horizontal stirrups and D10a50 stirrups, as illustrated in Fig. 1. For the flexural strengthening of the beams, four 2300 mm length CFRP strips of 1.4 mm (thickness) ×10 mm (depth) cross-sectional dimensions were applied using the NSM technique. Strips of two layers of EXB CFRP U-wraps of 60 mm width and 0.176 mm thickness at 150 mm spacing were applied to strengthen the beam SFS-I, as represented in Fig. 1(a). The exact number and distribution of strips of EXB CFRP U-wraps were adopted for shear strengthening of the beam SFS-II but implementing only one layer, as shown in Fig. 1(b).

Table 1. General information about the tested beams [16]

Group	Beam notation	ρ_{sl} (%)	ρ_{sw} (%)	CFRP flexural strengthening	CFRP shear strengthening		
				ρ_{fl} (%)	s_f (mm)	θ_f (°)	ρ_{fw} (%)
Group I	REF-I	1.46 (3D20)	0.10 (D6a300)	-	-	-	-
	SFS-I			0.08[a]	150[b]	90	0.16
Group II	REF-II	1.74 (2D20+1D25)	0.21 (D6a150)	-	-	-	-
	SFS-II			0.08[a]	150[c]	90	0.08

[(a)] NSM CFRP strips; [(b)] Strips of EXB CFRP U-wraps – 2 layers; [(c)] Strips of EXB CFRP U-wraps – 1 layer.

Table 2. Mechanical properties of materials used [16]

Concrete	Mean compressive strength f_{cm} (MPa) 44.3		Mean elastic modulus E_{cm} (GPa) 34.1
Steel reinforcement	Diameter D (mm)	Yield tensile stress f_y (MPa)	Ultimate tensile strength f_u (MPa)
	D6	641	737
	D20	636	767
	D25	657	790
CFRP strips	Tensile strength f_{fu} (MPa)	Elastic modulus E_{fu} (GPa)	Ultimate strain ε_{fu} (‰)
	3165	175	18.0
CFRP sheets	Tensile strength f_{fu} (MPa)	Elastic modulus E_{fu} (GPa)	Ultimate strain ε_{fu} (‰)
	3096	245	12.6

Table 1 shows that the tested beams had percentages of longitudinal tension reinforcement (ρ_{sl}) of 1.46% and 1.74%, percentages of steel stirrups (ρ_{sw}) of 0.1% to 0.21%, percentages of NSM CFRP strips (ρ_{fl}) of 0.08%, and percentages of EXB CFRP sheets (ρ_{fw}) of 0.08% and 0.16% for the beams in the group I and group II, respectively. Table 2 provides the material properties used in the experimental work [16].

2.2. *General description and material modeling*

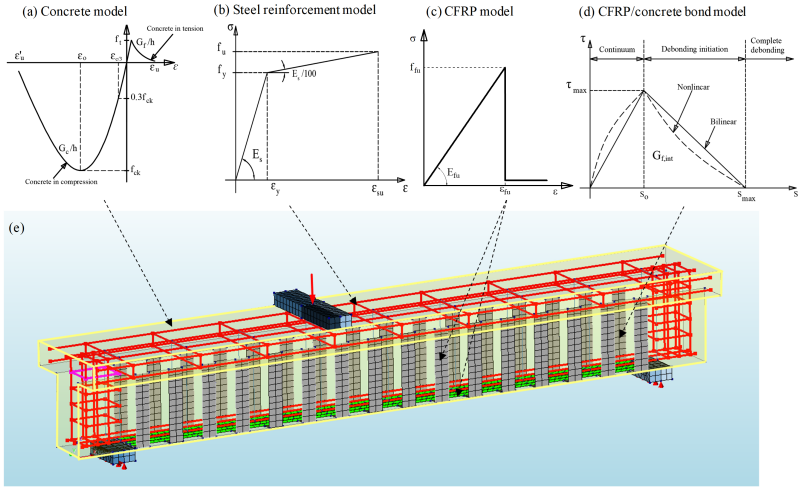

Figure 2. Finite element model of the strengthened T-beam: (a) Concrete under tension and compression; (b) Steel reinforcement; (c) NSM CFRP strips and EXB CFRP sheets; (d) Bond-slip of CFRP/concrete interface

A nonlinear three-dimensional finite element method was developed to simulate the behavior of RC T-beams strengthened with a CFRP system combined by NSM strips and U-wrap sheets subjected to asymmetric loading using DIANA software [27]. The analysis was conducted by incrementing displacement on the loading point in step until failure occurs. Fig. 2 shows the finite element model of SFS-type beams used in the validation study presented in the following section.

Concrete is modeled through a total-strain-based rotating smeared crack model using the CHX60 elements. The mechanical behavior of the concrete was simulated by stress-strain curves in compression and tension, as shown in Fig. 2(a) [28]. The compressive strength (f_{cm}) and modulus of elasticity of the concrete on the testing day are 44.3 MPa and 34.1 GPa, respectively [16]. If the test results were unavailable, the tensile strength (f_t) and modulus of elasticity of the concrete can be determined as suggested by *fib* Model Code 2010 [29]. The tensile fracture energy of concrete (G_f) was taken as 0.039 Nmm/mm, calculated according to Eq. (1), where G_{fo} is the base value of the fracture energy, taken as 0.035 for coarse aggregate with $d_{\max}$ = 19 mm, while f_{cmo} was taken as 10 MPa. Meanwhile, the compressive failure energy of concrete (G_c) is calculated according to Eq. (2) proposed by Nakamura and Higai [30] and is taken as 9.8 Nmm/mm^2. The crack width range was noted as h, equal to $\sqrt[3]{V}$, where V is the block element volume.

$$G_f = G_{fo}\left(\frac{f_{cm}}{f_{cmo}}\right)^{0.7} \tag{1}$$

$$G_c = 250 G_f \tag{2}$$

Steel rebars consisting of top and bottom longitudinal reinforcements and transverse reinforcement are modeled with one-dimensional truss elements embedded in concrete elements, corresponding to a perfect bond between reinforcement and concrete. The stress-strain behavior of steel reinforcement, as shown in Fig. 2(b), was simulated by two curves as follows:

$$f_s = \begin{cases} E_s\varepsilon_s & \text{for } \varepsilon_s \le \varepsilon_y \\ f_y + 0.01E_s(\varepsilon_s - \varepsilon_y) & \text{for } \varepsilon_s > \varepsilon_y \end{cases} \quad (3)$$

where f_y is the yield strength; ε_y is the yield stress ($\varepsilon_y = f_y/E_s$); E_s is Young's modulus, taken as 200 GPa.

The NSM CFRP strips for flexural strengthening were simulated using the CQ40S element, which is a quadrangular isotropic curved shell element with eight nodes. The mechanical behavior of CFRP, modeled by a linear relationship between stress and strain under tension, as shown in Fig. 2(c), is taken from the experimental work [16] (see Table 2). The stress value upon failure is reduced to a small value (instead of 0) to allow for stress redistribution upon failure. The interaction between the NSM CFRP strips and the concrete is modeled as a perfect bond. Meanwhile, the strips of CFRP U-wraps for shear strengthening were also simulated using CQ40S elements with a thickness (t_f) of 0.176 mm.

The adhesive layer between the EXB CFRP and the concrete was simulated by CQ48I elements, which had a zero thickness. In this study, the adhesion property was determined using the theoretical model proposed by Lu et al. [31], as shown in Fig. 2(d). The shear stress (τ) and bond slip (S) at the interface between EXB CFRP and concrete recommended by Lu et al. [31] were recently used in finite element analysis. The parameters and equation details of the theoretical model have been presented previously [13, 15, 18] and are not repeated herein. The maximum shear stress (τ_{max}) was calculated as a function of the ratio β_w between the CFRP width (b_f) and the concrete beam width (b_c), while the tensile strength of the concrete (f_t) was calculated based on the compressive strength. Since the EXB CFRP sheets were attached to both sides of the concrete beam, the width b_f was assumed to be 60 mm, and the width b_c was assumed to be 300 mm, which is equal to the distance from the bottom of the beam to the bottom edge of the T-flange. Therefore, the maximum shear stress is 4.56 MPa. The delamination process began when the tensile stress at the EXB CFRP/concrete interface exceeded the maximum shear stress.

The steel plates at the loading point and two supports were modeled by CHX60 elements. The material properties of the steel plates are modeled with an elastic modulus of 200 GPa, and Poisson's coefficient is taken as 0.3.

3. NLFE model validation

Four T-beams presented above were utilized to validate the proposed finite element model. The influence of concrete element mesh size on simulation results was investigated with sizes of 25 mm, 35 mm, and 50 mm. The results show that the 50×50×50 mm element mesh size provides a reasonable accuracy similar to the 25×25×25 mm element mesh size but allows to save more time and computer resources. Therefore, the uniform rectangular mesh size of 50×50×50 mm was selected for modeling. Figs. 3(a) and 3(b) illustrate the predicted and measured applied load-displacement curves for those T-beams, respectively. It can be observed from FE results that those T-beams exhibited behavior during loading similar to the experiments. The flexural cracks developed first at the bottom near the load section. As the displacement increased, these cracks became wider and propagated deep into the section, and new flexural and flexural-shear cracks appeared along the two shear spans of the T-beams. When the typical shear failure crack appeared, the load-carrying capacity reduced considerably, so the

test/simulation was stopped. Generally, the overall trend of the applied load-displacement curve of the T-beams derived by the proposed FE model was captured quite well with measured experimental data. The maximum load corresponding to the highest load value was predicted with reasonable accuracy. The difference between the predicted and experimental results in terms of maximum load is less than 7%, as shown in Table 3. The difference between numerical predictions and measured data can be attributed to variations arising from material models, which may differ from actual material models, as well as geometry, longitudinal steel position, loading, and support conditions.

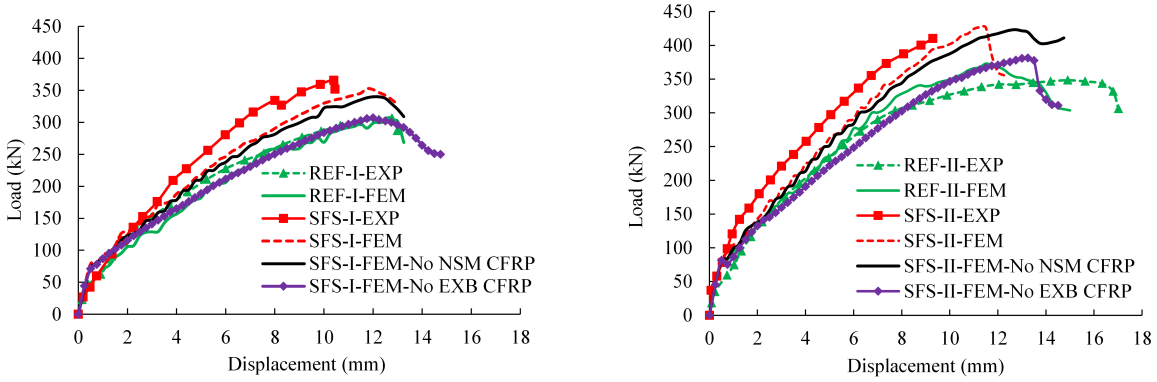

(a) Group I (b) Group II

Figure 3. Comparison of applied load-displacement curves between experiment and FEA

Table 3. Comparison of the ultimate load between experiment and FEA

Group	Beam notation	Ultimate load		Difference[(a)] (%)	Failure mode
		$P_{u,EXP}$ (kN)	$P_{u,FEM}$ (kN)		
Group I	REF-I	310.3	303.7	−2.1	Shear
	SFS-I	365.1	352.7	−3.4	Debonding/Shear
	SFS-I-No NSM CFRP	-	339.9	-	Debonding/Shear
	SFS-I-No EXB CFRP	-	307.1	-	Shear
Group II	REF-II	349.5	372.9	6.7	Shear
	SFS-II	411.4	426.9	3.7	Debonding/Shear
	SFS-II-No NSM CFRP	-	423.2	-	Debonding/Shear
	SFS-II-No EXB CFRP	-	381.1	-	Shear

[(a)] Difference (%) = $[(P_{u,FEM} - P_{u,EXP})/P_{u,EXP}]\times 100$.

Table 3 compares the ultimate load values between experimental and FE results for two control beams (REF-I and REF-II) and two strengthened beams (SFS-I and SFS-II). In order to explore and separate the effectiveness of NSM CFRP strips for flexural strengthening and EXB CFRP sheets for shear strengthening, two additional FE models in each specimen group (four beams in total) were conducted. The FE-applied load-displacement curves are shown in Fig. 3. The nomenclatures of SFS-I-FEM-No NSM CFRP and SFS-II-FEM-No NSM CFRP beams indicate that these two beams are similar to the two beams SFS-I and SFS-II, respectively except that the NSM CFRP strips for flexural strengthening were removed as expressed by No NSM CFRP at the end of the beam names. At the same time, the two beams named SFS-I-FEM-No EXB CFRP and SFS-II-FEM-No EXB CFRP show

that these two beams are similar to the two beams SFS-I and SFS-II, but they do not have the EXB CFRP sheets for shear strengthening as denoted by No EXB CFRP at the end of the beam names.

Considering the effect of NSM CFRP strips, it is apparent from Fig. 3 that eliminating flexural reinforcement with CFRP strips is shown to slightly lower the post-cracking stiffness and bearing capacity of the two beams SFS-I-FEM-No NSM CFRP and SFS-II-FEM-No NSM CFRP in comparison with SFS-I-FEM and SFS-II-FEM, respectively. Specially, bearing capacity of SFS-I-FEM-No NSM CFRP was reduced by 5.7% compared with that of SFS-I-FEM, while bearing capacity of SFS-II-FEM-No NSM CFRP was reduced by 0.9% compared with that of SFS-II-FEM. The two beams (SFS-I-FEM-No NSM CFRP and SFS-II-FEM-No NSM CFRP) were also predicted to fail in shear initiated by debonding of EXB-CFRP sheets.

Comparing the ultimate loads between REF-I-FEM and SFS-I-FEM-No NSM CFRP showed that the two layers of EXB CRFP sheets effectively increase the bearing capacity by 12.0%. Meanwhile, one layer of EXB CRFP sheets effectively increases the bearing capacity by 13.5% compared to REF-II-FEM and SFS-II-FEM-No NSM CFRP. This phenomenon indicates the usefulness of EXB CFRP sheets in enhancing the bearing capacity of the T-beams. However, it is worth noting that the amount of steel stirrups and longitudinal tension steel in the latter cases is higher than that of the first two beams.

Regarding the effect of EXP CFRP strips, it is observed from Fig. 3 that the beams eliminating EXB CFRP sheets (SFS-I-FEM-No EXB CFRP and SFS-II-FEM-No EXB CFRP) exhibit quite similar behavior with comparable beams without EXB CFRP sheets (REF-I-FEM and REF-II-FEM). For a given amount of longitudinal tension steels and stirrups, removing EXB CFRP sheets had no or some small effect on the bearing capacity, probably due to the dominant influence of the typical diagonal shear failure crack due to over-reinforced concrete beams originally. Comparing the ultimate loads between REF-I-FEM and SFS-I-FEM-No EXB CFRP showed that the NSM CRFP strips only enhanced the bearing capacity by 1.1%. The NSM CRFP strips only improve the bearing capacity by 2.1% compared to the ultimate loads between REF-II-FEM and SFS-II-FEM-No EXB CFRP.

Fig. 4 compares the predicted strain contour at the end of the simulation and the observed crack pattern for experimental specimens. For control beams (REF-I and REF-II), it is seen that due to the asymmetric loading, typical diagonal shear failure cracks in the web region appeared only on the left side from the supports to the point of force application where higher shear stress appeared, which is consistent with the experimental beams, as shown in Figs. 4(a) and 4(b). The reason for shear failure was mainly attributed to the inadequate transverse reinforcement provided. For strengthened beams (SFS-I and SFS-II), the experimental results showed the same failure mode as the experimental results, which was the debonding of the EXB CFRP sheets crossed by inclined shear cracks, as shown in Figs. 4(c) and 4(d). The tensile stress at the EXB CFRP sheet /concrete interface exceeded the maximum bond stress.

The proposed FE model is capable of tracing the progression of strains at any element in the T-beam. Fig. 5 shows the relationship between the applied load and the strains in the strain gauges positioned in the monitored EXB CFRP sheet (SG_CV4), NSM CFRP strip (SG_CL2), and longitudinal steel bar (SG_SL), respectively, for the verified beams of groups I and II. It is apparent that strain predictions are in good agreement with measured strain data. Due to a malfunction in the experiment, the strain of longitudinal tension reinforcement was not recorded for beam SFS-II. Therefore, it was not expressed in Fig. 5. The FE results reveal that the yielding of longitudinal reinforcements has not yet occurred. Furthermore, the NSM CFRP strips were still in the elastic range, and no rupture of the NSM CFRP strips was observed in both experimental and FE results.

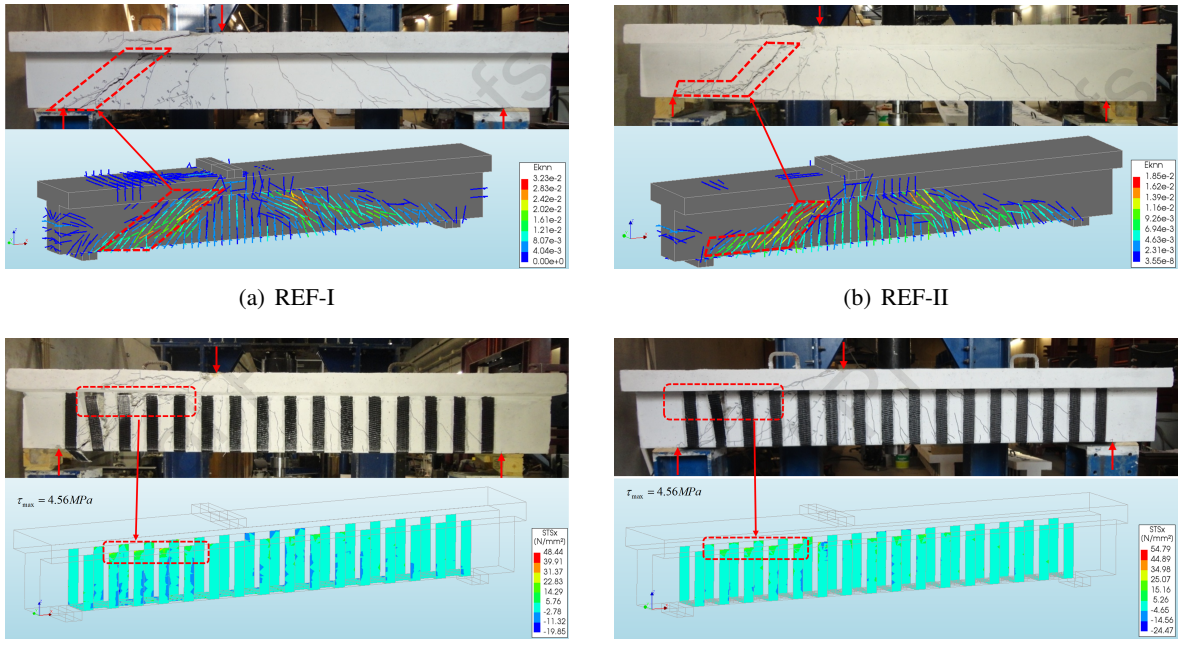

(a) REF-I (b) REF-II

(c) SFS-I (d) SFS-II

Figure 4. Comparison of failure modes between experiment and FEA

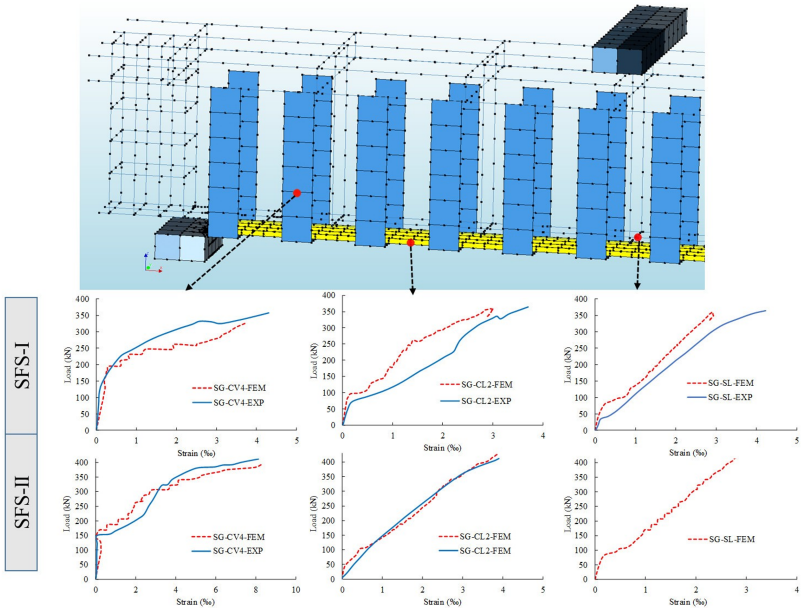

Figure 5. Comparison of variation of strains in the monitored CFRPs and steel between experiment and FEA: (a) SFS-I; (b) SFS-II

4. Parametric investigations and discussions

The successfully developed FE model, as presented above, has been used in a parametric study to investigate critical parameters affecting the performance of T-beams strengthened with NSM strips and U-wraps, including (i) concrete compressive strength, (ii) amount of longitudinal tension rein-

forcement, (iii) amount of stirrups, (iv) multiple layers of EXB CFRP sheets, and (v) T-shape width. The SFS-I beam model was used to develop a series of FE models to investigate those parameters. The concrete compressive strength ranged from 30 MPa to 50 MPa. The amount of longitudinal tension reinforcement varied by changing the diameter from 16 mm to 25 mm. The amount of stirrups varied by changing the spacing of stirrups from 100 mm to 300 mm. The layers of U-wraps ranged from two to five layers. Each parameter had three to four discrete levels. Table 4 summarizes the FE analyses in this section.

Table 4. Summary of results from FEA

Beam notation	Ultimate load, P_{max} (kN)	Displacement* (mm)	Failure mode
SFS-I-B30	274.1	12.5	Debonding/Shear
SFS-I-B35	302.7	13.0	Debonding/Shear
SFS-I-B44.3	352.7	11.8	Debonding/Shear
SFS-I-B50	395.5	13.5	Debonding/Shear
SFS-I-D16	330.0	16.8	Flexure-Shear
SFS-I-D18	345.9	15.8	Flexure-Shear
SFS-I-D20	352.7	11.8	Debonding/Shear
SFS-I-D25	356.8	9.3	Debonding/Shear
SFS-I-a300	352.7	11.8	Debonding/Shear
SFS-I-a250	387.3	12.8	Debonding/Shear
SFS-I-a150	424.7	12.8	Flexure-Shear
SFS-I-a100	439.3	12.3	Flexure-Shear
SFS-I-2L	352.7	11.8	Debonding/Shear
SFS-I-3L	362.2	11.8	Debonding/Shear
SFS-I-4L	369.4	12.3	Debonding/Shear
SFS-I-5L	373.0	12.5	Debonding/Shear
SFS-I-180	258.5	11.3	Debonding/Shear
SFS-I-400	352.7	11.8	Debonding/Shear
SFS-I-580	382.7	12.0	Flexure-Shear
SFS-I-720	393.5	14.0	Flexure-Shear

* Displacement corresponding to the ultimate load.

4.1. Effect of concrete compressive strength

Four strengthened T-beams, which are constructed based on the original SFS-I beams denoted as SFS-I-B30, SFS-I-B35, SFS-I-B44.3, SFS-I-B50 corresponding to the concrete compressive strengths of 30 MPa, 35MPa, 44.3 MPa, and 50 MPa, respectively, were analyzed to investigate the influence of concrete on the bearing capacity of the strengthened beams. Fig. 6 shows the effect of the concrete compressive strength on the applied load-displacement curves of the beams from FE models. It is seen that the load-carrying capacity was positively affected as the concrete compressive strength increased. The increase in the bearing capacity of the model beams may be due to an increase in the shear resistance of the concrete as the shear strength of the concrete increases, owing to the increase in the compressive strength of the concrete. Furthermore, as the concrete compressive strength increased, the stiffness of the beam was also increased. Results from numerical modeling show that shear failure of reinforced beams occurs with the debonding of CFRP along with the appearance of typical inclined

failure cracks. Concrete compressive strength had little effect on the displacements corresponding to the maximum applied load of the beams (see Table 4).

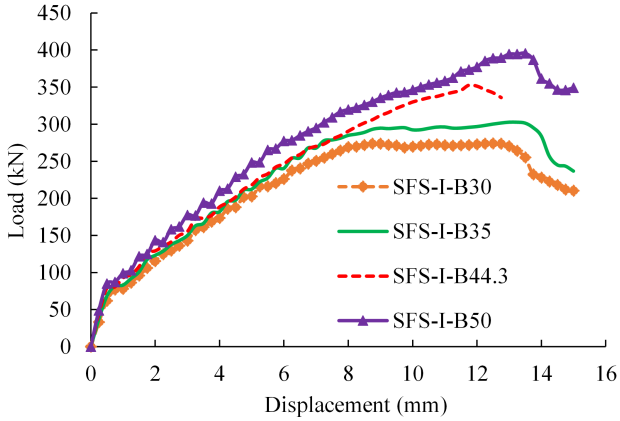

Figure 6. Effect of concrete compressive strength on the applied load-displacement relationship

4.2. Effect of amount of longitudinal tension reinforcement

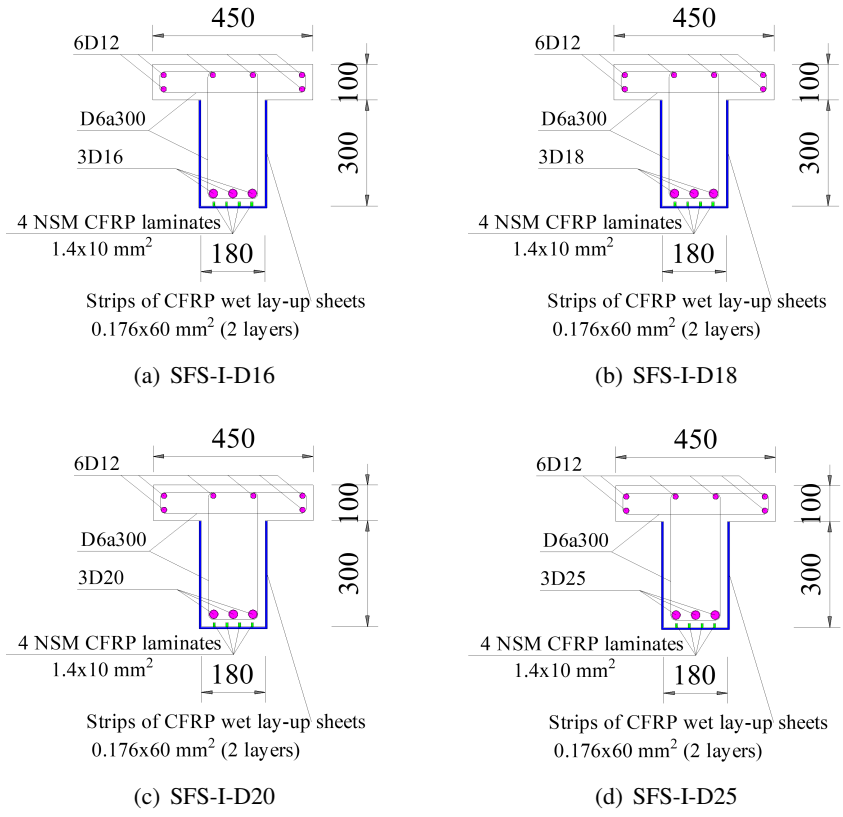

Figure 7. Cross-section of strengthened T-beams with various diameters of longitudinal tension reinforcement

In this section, three models have been developed based on the SFS-I beam model, which can be expressed as SFS-I-D20, to investigate the effect of the amount of longitudinal tension reinforcement

on the bearing capacity of the strengthened T-beam. Three beam models designated as SFS-D16, SFS-D18, and SFS-D25 used the same type of concrete as beam SFS-I-D20 and are arranged with three longitudinal tension reinforcement bars with diameters ranging from 16 mm to 18 mm and 25 mm, as shown in Fig. 7. These models have the same reinforcement arrangement on the T-flange similar to the SFS-I-D20 beam.

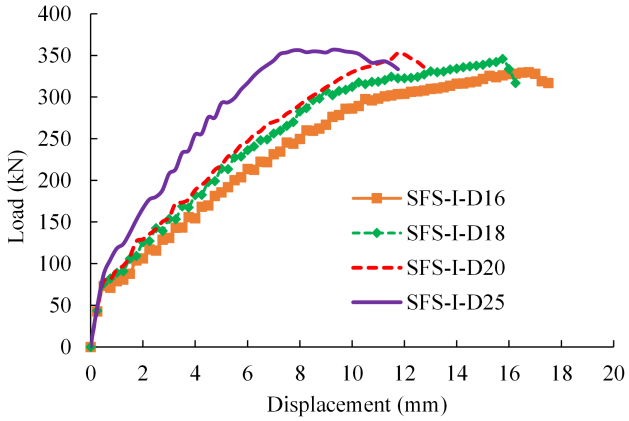

Figure 8. Effect of amount of longitudinal tension reinforcement on the applied load-displacement relationship

Fig. 8 shows the applied load-displacement curves of strengthened T-beams with various amounts of longitudinal tension reinforcement. It is observed that increasing longitudinal tension reinforcement had no or minor degree of positive effect on the load-displacement curve prior to the concrete crack. After concrete cracking, increasing the longitudinal tension reinforcement ratio causes a pronounced increase in the load capacity of the T-beams. However, the higher longitudinal tension reinforcement ratio also results in less ductile behavior for the T-beams (see Table 4 and Fig. 8). It can be explained that for a given shear capacity, increasing the longitudinal tension reinforcement ratio reduces the development of the tensile strain of the longitudinal reinforcement, thereby reducing the displacement of the beam. Based on the given amount of stirrups and EXB CFRP sheets, the numerical results reveal that reduction of longitudinal tension reinforcement from diameter of 20 mm to equal or lower than 18 mm could shift the failure mode from shear failure as evidenced by the occurrence of major shear crack to flexural-shear failure when yielding of longitudinal reinforcement was firstly initiated and followed by debonding of EXB CFRP and appearance of typical inclined shear crack at the end of the simulation. Longitudinal tension reinforcement of the beams SFS-I-D20 and SFS-I-D25 have not yet yielded, whereas that of SFS-I-D16 and SFS-I-D18 yielded at displacement of 10.5 mm and 13.75 mm, respectively.

4.3. Effect of amount of stirrups

In this section, four beam models are designated as SFS-I-a300, SFS-I-a250, SFS-I-a150, and SFS-I-a100 corresponding to the stirrup spacing of 300 mm, 250 mm, 150 mm, and 100 mm, developed from the original SFS-I beam to investigate the beam's behavior. The amount of stirrups varies with the change in their spacing. Fig. 9 illustrates the cross-section of T-beams with different spacings between stirrups. Fig. 10 shows the load-displacement curves obtained from the FEA of the beams above. Firstly, for a given amount of longitudinal tension reinforcement, as reducing the stirrups spacing from 250 mm to 150 mm, the failure mode of the beam changes from debonding of EXB CFRP along with diagonal cracking to flexural-shear failure as yielding of vertical steel reinforcement occurs, and finally, diagonal cracking appears. Furthermore, as expected, reducing the stirrups spacing

increases the load-carrying capacity of the beam (see Fig. 10 and Table 4). This can be explained by the fact that reducing the spacing between stirrups increases the ability to resist the formation of inclined cracks due to shear forces, thus increasing the load-bearing capacity. The flexibility (displacement) of the beam tends to increase when the spacing between stirrups is reduced from 300 mm to 150 mm. However, the flexibility of the beam tends to decrease when the spacing between stirrups is reduced from 150 mm to 100 mm. The beam with a stirrups spacing of 100 mm is still more ductile than that with a spacing of 300 mm (see Table 4).

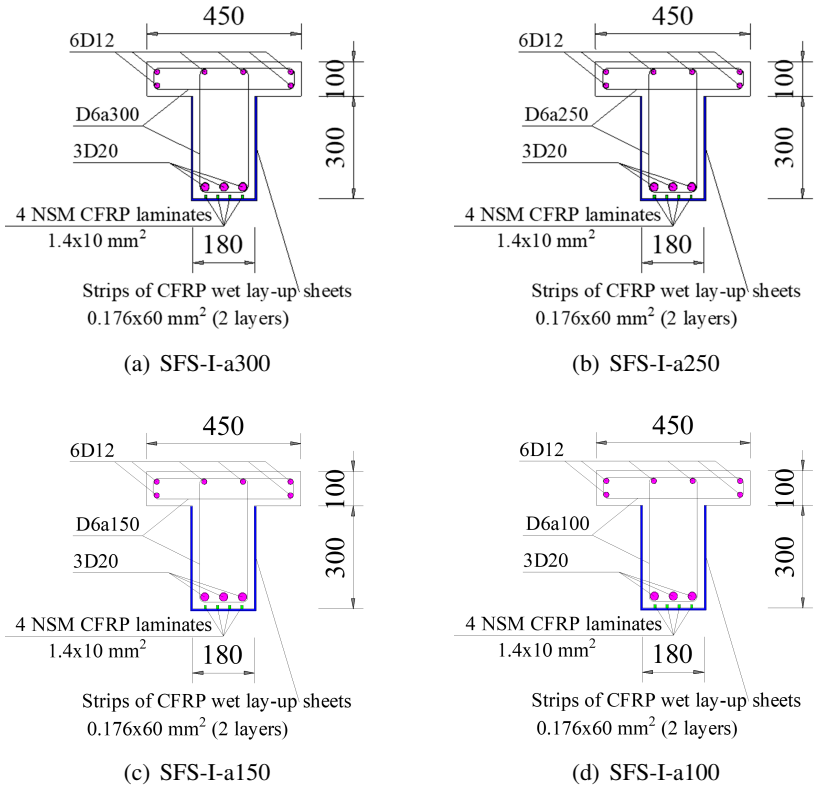

Figure 9. Cross-section of strengthened T-beams with various spacing of stirrups

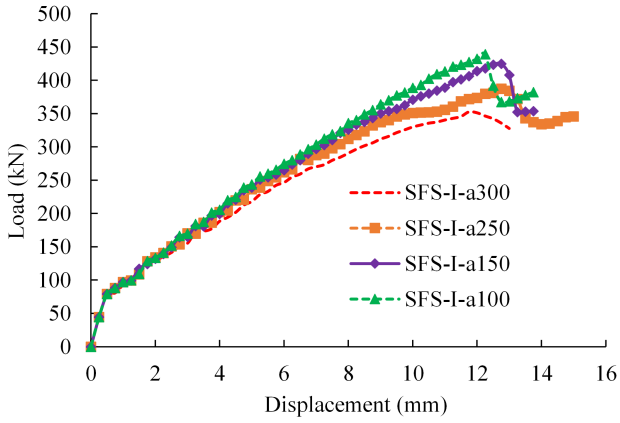

Figure 10. Effects of amount of stirrups on the applied load-displacement relationship

4.4. Effect of multiple CFRP layers

In this section, four beam models with multiple layers of EXB CFRP sheets (U-wraps) are investigated. These models, namely SFS-I-2L, SFS-I-3L, SFS-I-4L, and SFS-I-5L, correspond to beams with 2, 3, 4, and 5 layers of EXB CFRP, respectively. They are developed from the original SFS-I beam to study the beam's behavior. Fig. 11 illustrates the cross-section of T-beams with multiple layers of U-wraps. Fig. 12 shows the applied load-displacement curves of the beams obtained through FEA. All model beams experienced failure due to shear and delamination of CFRP layers. It can be

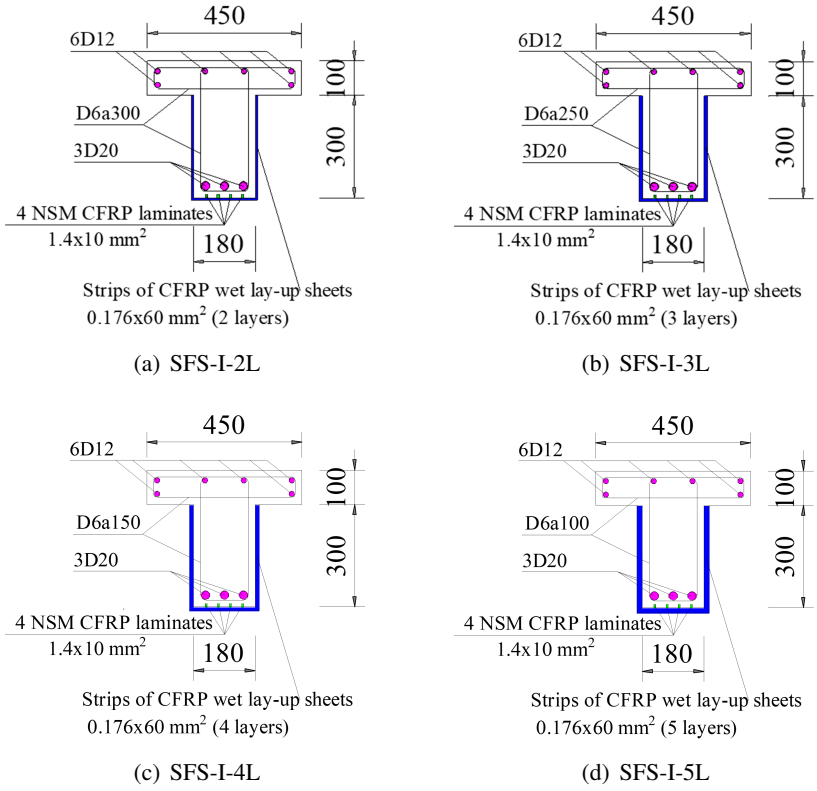

Figure 11. Cross-section of strengthened T-beams with multiple layers of U-wraps

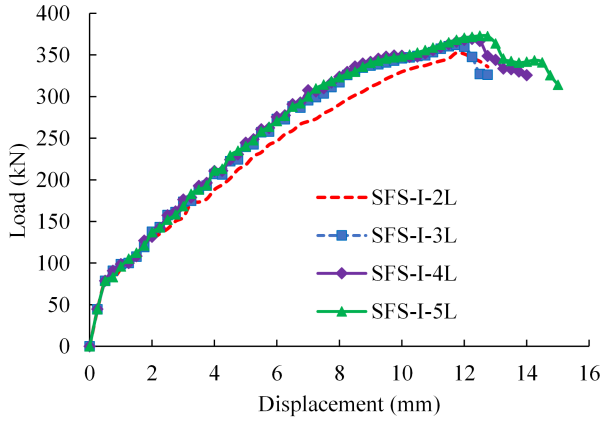

Figure 12. Effect of multiple CFRP layers on the applied load-displacement relationship

observed that increasing the number of CFRP layers from 2 to 5 results in a maximum load increase of 5.8%. The higher the number of CFRP layers, the higher the load capacity of the beam. The flexibility (displacement) of the beams tends to increase as the number of CFRP layers increases (see Table 4 and Fig. 12). Increasing the number of CFRP layers enhances the shear resistance of the beam to withstand the applied load. The increase in shear resistance improves the ability of the section to mobilize the strain in the longitudinal reinforcement; therefore, the applied load and ductility of the beam increase.

4.5. Effect of flange width

In this section, four beam models are designated as SFS-I-180, SFS-I-450, SFS-I-580, and SFS-I-720, corresponding to flange widths of 180 mm, 450 mm, 580 mm, and 700 mm, respectively, to investigate the influence of T-shaped on the shear behavior of the beams, as shown in Fig. 13. These beams are developed from the original SFS-I beam. Fig. 14 shows the applied load-displacement curve obtained from the FEA of four beam models. The results indicate that increasing the flange width increases the load-bearing capacity of the beam. The increase in load-bearing capacity of the beam can be explained by the increase in cross-sectional area subjected to shear, thus increasing the shear capacity of the concrete and the beam. Therefore, the failure mode of the beam changes from shear failure when the flange width is less than 450 mm to flexural-shear failure when the longitudinal steel reinforcement has yielded, resulting in CFRP debonding and formation of inclined cracks with a flange width greater than 580 mm. Furthermore, it can be observed that as the flange width increases, the flexibility of the beam also increases (see Table 4).

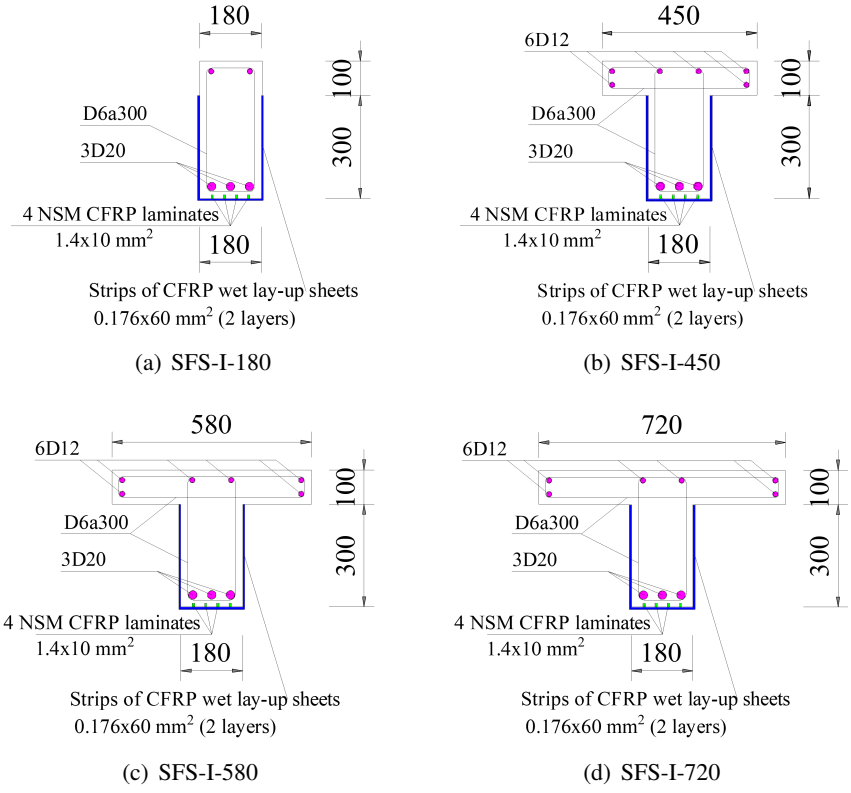

Figure 13. Cross sections of strengthened beams with various widths of flange

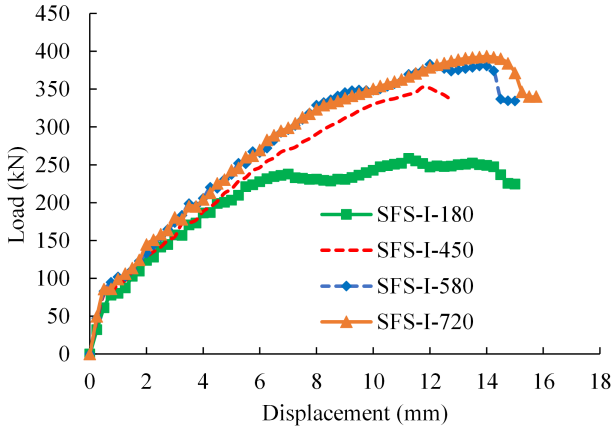

Figure 14. Effect of flange width on the applied load-displacement relationship

5. Conclusions

This study presents a developed finite element model to simulate the behavior of RC T-beams strengthened in flexural and shear capacity using near-surface mounted strips and externally bonded U-wraps. The beams were subjected to asymmetric three-point loading. Based on the results obtained from validation and parametric investigations, the main conclusions are summarized as follows:

- From the validation section, it is clearly seen that the developed finite element model can provide a reasonable prediction of the behavior of the tested beams with and without CFRP flexural and shear strengthening in terms of applied load-displacement curves and failure modes.

- Some conclusions were derived from parametric investigations. Mechanical explanations of these observations are presented and discussed.

+ Increasing the concrete strength will increase the applied load of the strengthened T-beam. However, it was found that the concrete strength has a minor effect on the displacement of the beam studied in this work.

+ As the amount of vertical steel reinforcement increases, it has no or minimal effect on the load-bearing capacity of the strengthened T-beam. However, the beam failure transitions from a shear mode (with CFRP debonding) to a flexural-shear mode (with ductile yielding of the longitudinal tension reinforcement). The higher the amount of longitudinal tension reinforcement, the lower the flexibility of the beam.

+ Increasing the amount of stirrups tends to improve the applied load and ductility of the strengthened T-beam considered in this study.

+ The higher the number of CFRP layers, the higher the load capacity and ductility of the strengthened T-beam considered in this study.

+ Increasing the flange width enhances the load-bearing capacity and flexibility of the strengthened T-beam. As the flange is less than 450 mm, the failure mode of the beam is due to the formation of major shear cracks. As the flange is greater than 580 mm, the failure mode changes to flexure-shear due to the yielding of the longitudinal tension reinforcement accompanied by EXB CFRP debonding.

References

[1] Ou, Y.-C., Nguyen, N. D. (2016). Influences of location of reinforcement corrosion on seismic performance of corroded reinforced concrete beams. *Engineering Structures*, 126:210–223.

[2] Ou, Y.-C., Nguyen, N. D. (2016). Modified axial-shear-flexure interaction approaches for uncorroded and corroded reinforced concrete beams. *Engineering Structures*, 128:44–54.

[3] Mugahed Amran, Y. H., Alyousef, R., Rashid, R. S. M., Alabduljabbar, H., Hung, C.-C. (2018). Properties and applications of FRP in strengthening RC structures: A review. *Structures*, 16:208–238.

[4] Naser, M. Z., Hawileh, R. A., Abdalla, J. A. (2019). Fiber-reinforced polymer composites in strengthening reinforced concrete structures: A critical review. *Engineering Structures*, 198:109542.

[5] Siddika, A., Mamun, M. A. A., Ferdous, W., Alyousef, R. (2020). Performances, challenges and opportunities in strengthening reinforced concrete structures by using FRPs – A state-of-the-art review. *Engineering Failure Analysis*, 111:104480.

[6] Dong, J., Wang, Q., Guan, Z. (2013). Structural behaviour of RC beams with external flexural and flexural–shear strengthening by FRP sheets. *Composites Part B: Engineering*, 44(1):604–612.

[7] Siddika, A., Mamun, M. A. A., Alyousef, R., Amran, Y. M. (2019). Strengthening of reinforced concrete beams by using fiber-reinforced polymer composites: A review. *Journal of Building Engineering*, 25: 100798.

[8] Elsanadedy, H. M., Abbas, H., Almusallam, T. H., Al-Salloum, Y. A. (2019). Organic versus inorganic matrix composites for bond-critical strengthening applications of RC structures – State-of-the-art review. *Composites Part B: Engineering*, 174:106947.

[9] Mai, A. D., Sheikh, M. N., Yamakado, K., Hadi, M. N. S. (2020). Nonuniform CFRP Wrapping to Prevent Sudden Failure of FRP Confined Square RC Columns. *Journal of Composites for Construction*, 24(6).

[10] Valerio, P., Ibell, T. J., Darby, A. P. (2009). Deep embedment of FRP for concrete shear strengthening. *Proceedings of the Institution of Civil Engineers - Structures and Buildings*, 162(5):311–321.

[11] Ke, Y., Zhang, S. S., Smith, S. T., Yu, T. (2023). Novel Embedded FRP Anchor for RC Beams Strengthened in Flexure with NSM FRP Bars: Concept and Behavior. *Journal of Composites for Construction*, 27 (1).

[12] Tran, C. T. N., Nguyen, X. H., Nguyen, H. C., Le, D. D. (2021). Shear performance of short-span FRP-reinforced concrete beams strengthened with CFRP and TRC. *Engineering Structures*, 242:112548.

[13] Tan, N. N., Kien, N. T., Giang, N. H. (2021). Numerical study on the flexural performance of RC beams with externally bonded CFRP sheets. *Journal of Science and Technology in Civil Engineering (STCE) - HUCE*, 15(4):182–196.

[14] Anh, T. H., Giang, N. H., Tan, N. N. (2021). An experimental study on the flexural strengthening of corroded RC beams using externally CFRP sheet. *Journal of Science and Technology in Civil Engineering (STCE) - HUCE*, 15(1V):1–16. (in Vietnamese).

[15] Nguyen, N. T., Nguyen, T. K., Du, D. H., Nguyen, D. N., Kieu, T. S. (2023). Nonlinear finite element analysis of FRP-strengthened full-size reinforced concrete beams. *Innovative Infrastructure Solutions*, 8 (5).

[16] Dias, S. J. E., Silva, J. R. M., Barros, J. A. O. (2021). Flexural and shear strengthening of reinforced concrete beams with a hybrid CFRP solution. *Composite Structures*, 256:113004.

[17] Jin, L., Jiang, X., Lu, K., Du, X. (2022). Tests on shear failure and size effect of CFRP-wrapped RC beams without stirrups: Influence of CFRP ratio. *Composite Structures*, 291:115613.

[18] Nguyen, N. T., Nguyen, T. K., Du, D. H., Nguyen, D. N. (2022). Finite-Element Analysis of RC Beams Strengthened With CFRP U-Wraps. *Mechanics of Composite Materials*, 58(4):567–584.

[19] AlHamaydeh, M., Markou, G., Bakas, N., Papadrakakis, M. (2022). AI-based shear capacity of FRP-reinforced concrete deep beams without stirrups. *Engineering Structures*, 264:114441.

[20] Elghandour, B., Eltahawy, R., Shedid, M., Abdelrahman, A. (2023). Prediction of shear strength for CFRP reinforced concrete beams without stirrups. *Engineering Structures*, 284:115946.

[21] Askar, M. K., Hassan, A. F., Al-Kamaki, Y. S. S. (2022). Flexural and shear strengthening of reinforced concrete beams using FRP composites: A state of the art. *Case Studies in Construction Materials*, 17: e01189.

[22] Nikoloutsopoulos, N., Passa, D., Gavela, S., Sotiropoulou, A. (2018). Comparison of shear strengthening techniques of reinforced concrete beams with carbon fibre reinforced polymers (CFRPs). *Procedia Structural Integrity*, 10:141–147.

[23] Godat, A., Hammad, F., Chaallal, O. (2020). State-of-the-art review of anchored FRP shear-strengthened RC beams: A study of influencing factors. *Composite Structures*, 254:112767.

[24] Osman, B. H., Wu, E., Ji, B., Abdulhameed, S. S. (2018). Effect of reinforcement ratios on shear behavior of concrete beams strengthened with CFRP sheets. *HBRC Journal*, 14(1):29–36.

[25] Naser, M. Z., Hawileh, R. A., Abdalla, J. (2021). Modeling Strategies of Finite Element Simulation of Reinforced Concrete Beams Strengthened with FRP: A Review. *Journal of Composites Science*, 5(1):19.

[26] Njoko, F. H., Tambusay, A., Jamieson, A., Suryanto, B., Suprobo, P. (2023). Modelling of Shear-critical, Lightly Reinforced Concrete T-beams with Externally Bonded CFRP using ATENA Science. *Civil Engineering Dimension*, 25(2):67–77.

[27] Ferreira, D., Manie, J. (2020). *DIANA Documentation release 10.3*. DIANA FEA bv, 2020.

[28] Hordijk, D. A., Reinhardt, H. W. (1993). Numerical and experimental investigation into the fatigue behavior of plain concrete. *Experimental Mechanics*, 33(4):278–285.

[29] Model Code 2010. *fib Model Code for Concrete Structures 2010.* fib, Lausanne, 2013, pp. 40. Berlin, Germany: Wilhelm Ernst & Sohn.

[30] Nakamura, H., Higai, T. (2001). Compressive fracture energy and fracture zone length of concrete. In *Modeling of Inelastic Behavior of Rc Structures under Seismic Loads*, ASCE Publications, 471–487.

[31] Lu, X. Z., Teng, J. G., Ye, L. P., Jiang, J. J. (2005). Bond–slip models for FRP sheets/plates bonded to concrete. *Engineering Structures*, 27(6):920–937.